Electronic Research Archive

http://www.aimspress.com/journal/era

ERA, 30(7): 2618–2642.
DOI: 10.3934/era.2022134
Received: 24 July 2021
Revised: 15 December 2021
Accepted: 19 February 2022
Published: 16 May 2022

Research article

An improved coupled PDE system applied to the inverse image denoising problem

Abdelmajid El Hakoume, Lekbir Afraites and Amine Laghrib*

EMI FST Béni-Mellal, Université Sultan Moulay Slimane, Maroc

* **Correspondence:** Email: laghrib.amine@gmail.com.

Abstract: The problem of interest in this paper is the mathematical and numerical analysis of a new non-variational model based on a high order non-linear PDE system resulting from image denoising. This model is motivated by involving the decomposition approach of H^{-1} norm suggested by Guo et al. [1, 2] which is more appropriate to represent the small details in the textured image. Our model is based on a diffusion tensor that improves the behavior of the Perona-Malik diffusion directions in homogeneous regions and the Weickert model near tiny edges with a high diffusion order. A rigorous analysis of the existence and uniqueness of the weak solution of the proposed reaction-diffusion model is cheked in a suitable functional framework, using the Schauder fixed point theorem. Finally, we carry out a numerical result to show the effectiveness of our model by comparing the results obtained with some competitive models.

Keywords: image denoising; high order PDE system; anisotropic diffusion tensor; fixed point theorem

1. Introduction

Currently, Image restoration is one of the outstanding challenging problems in both image processing and computer vision with numberless applications. Its goal is to remove noise from a degraded image to restore the original one. Generally, given a noisy image function defined on Ω, with $\Omega \subset \mathbb{R}^2$ an open and bounded domain, the image denoising process can be modelled as $f = u + n$ where f represents the observed noisy image, u is the true image, and n is the noise component. To solve this inverse problem, there are several approaches such as PDE based technique [3, 4], wavelet based technique [5], stochastic approach [6], patch based technique [7].

PDE based denoising models can be classified in two categories, namely variational and non variational PDE models. In variational PDE models, the solution is obtained as the steady-state solution of an evolution equation corresponding to the Euler–Lagrange equation of the energy functional. In non-

variational PDE models, the PDE is proposed directly on the diffusion equations (systems), without thinking of any energy. Whatever the used approach, one should consider a certain diffusion equation (system).

In recent years, partial differential equations (PDEs) have become one of the most effective tools for image processing. Among them, the ROF model, which was first introduced by Rudin et al. [8], is one of the most popular and given by

$$\min_u E(u) = \int_\Omega |\nabla u| + \lambda \|u - f\|^2_{L^2(\Omega)}, \tag{1.1}$$

where $\lambda > 0$ is parameter regularization, $\|u - f\|^2_{L^2(\Omega)}$ is a fidelity term, and $\int_\Omega |\nabla u|$ is a regularization term. The corresponding PDE which the evolution of the Euler-Lagrange equation for $E(u)$ is given by following equation

$$\begin{cases} \frac{\partial u}{\partial t} = div\Big(\frac{\nabla u}{|\nabla u|}\Big) + 2\lambda(f - u) \ \ in \ \ \Omega, \\ \langle \nabla u, n\rangle = 0 \ \ on \ \ \partial\Omega, \end{cases} \tag{1.2}$$

This last model is named TV model, it has been the subject of several studies (see [9, 10]) and has successfully contributed to preserve edges during the restoration process. Given the success of TV-based diffusion, various modifications have been investigated (see [11, 12]). Though the TV model performs very well for image denoising and edge protecting, it may also destroy small details, such as textures (see [13]). To overcome this drawback, Meyer [14] proposed a new minimization method by introducing a weaker norm which is more appropriate to represent the oscillatory patterns and small details in the textured image. Subsequently, Osher et al. [13] proposed the following 4th order denoising model which used the H^{-1} norm with the TV minimization. The minimization energy has the form

$$\min E_{H^{-1}}(u) = \int_\Omega |\nabla u| + \lambda \|u - f\|^2_{H^{-1}(\Omega)}. \tag{1.3}$$

The corresponding PDE associated to Euler-Lagrange is given by the following equation :

$$\begin{cases} \frac{\partial u}{\partial t} = \Delta\Big(div\Big(\frac{\nabla u}{|\nabla u|}\Big)\Big) + 2\lambda(f - u) \ \ in \ \ \Omega, \\ \langle \nabla\Big(div(\frac{\nabla u}{|\nabla u|})\Big), n\rangle = \langle \nabla u, n\rangle = 0 \ \ on \ \ \partial\Omega, \end{cases} \tag{1.4}$$

This model is called the $TV - H^{-1}$ denoising model. This model is a highly nonlinear PDE and its numerical solution is not obvious. To solve this problem, Guo et al. [1] suggested a reaction-diffusion system applied to image restoration and image decomposition into cartoon and texture. This idea is introduced by [12] where the initial image f is decomposed into carton part u and texture or noise $(f - u)$. The Euler-Lagrange of the functional energy (1.3) becomes

$$\Delta^{-1}(f - u) = \frac{1}{2\lambda} div\Big(\frac{\nabla u}{|\nabla u|}\Big), \tag{1.5}$$

To overcome the difficulty of 4th order degrees in (1.5), the authors transform it into the following two coupled second order equations:

$$\begin{cases} -\Delta v + (f - u) = 0 \ \ in \ \ \Omega, \\ -div\Big(\frac{\nabla u}{|\nabla u|}\Big) + 2\lambda v = 0 \ \ in \ \ \Omega, \\ \langle \nabla u, n\rangle = \langle \nabla v, n\rangle = 0 \ \ on \ \ \partial\Omega, \end{cases} \tag{1.6}$$

and the evolutionary form of the steady system (1.6) is given by the following PDE system:

$$\begin{cases} \frac{\partial v}{\partial t} = \Delta v - (f-u) \ \ in \ \ \Omega \times (0,T), \\ \frac{\partial u}{\partial t} = div\Big(\frac{\nabla u}{|\nabla u|}\Big) - 2\lambda v \ \ in \ \ \Omega \times (0,T), \\ \langle \nabla u, n\rangle = \langle \nabla v, n\rangle = 0 \ \ on \ \ \partial\Omega \times (0,T), \\ u(0,x) = f \ \ in \ \ \Omega, \\ v(0,x) = 0 \ \ in \ \ \Omega. \end{cases} \tag{1.7}$$

Recently, Atlas et al. [15] proposed a new model based on a nonlinear fractional reaction-diffusion system. This model is based on the following minimization procedure:

$$\min E_{H^{-s}}(u) = \int_\Omega |\nabla u| + \lambda \|u - f\|^2_{H^{-s}(\Omega)}, \tag{1.8}$$

where the norm H^{-s}, $s > 0$ is introduced by Giga [16]. The corresponding PDE associated of its Euler-Lagrange will be

$$2\lambda(f-u) = (-\Delta)^s\Big(div\Big(\frac{\nabla u}{|\nabla u|}\Big)\Big). \tag{1.9}$$

where H^{-s} is negative Hilbert-Sobolev space with $s \in (0,1]$ For the nonlinear regularization term, the authors propose an Orlicz-operator and generalize Eq (1.9), which becomes:

$$2\lambda(f-u) = (-\Delta)^s\Big(div\Big(\frac{\mathcal{A}_{\mu(x)}(x,|\nabla|)\nabla u}{|\nabla u|}\Big)\Big). \tag{1.10}$$

where the function $A_{\mu(x)} : \Omega \times \mathbb{R} \to \mathbb{R}$ is chosen to be monotonically close to 1 when t tends to infinity (for more details see [15]). To solve the problem (1.10), the authors follow the decomposition suggested in [1, 2] introducing the following coupled system

$$\begin{cases} -div\Big(\frac{\mathcal{A}_{\mu(x)}(x,|\nabla|)\nabla u}{|\nabla u|}\Big) + 2\lambda v = 0, \\ (-\Delta)^s v + (f-u) = 0, \end{cases} \tag{1.11}$$

furthermore, the authors consider the solution (u, v) of system (1.11) as a steady state of an evolutionary fractional reaction-diffusion system investigated in [15].

More recently, Halim et al. [17] proposed a non-variational denoising model by modifying the $TV - TV2$ model introduced in [18]. They proposed the following model:

$$\frac{\partial u}{\partial t} = -\alpha\Delta\Big(div\Big(\frac{\nabla u}{|\nabla u|}\Big)\Big) + \beta\Big(div\Big(\frac{\nabla u}{|\nabla u|}\Big)\Big) + \lambda(f-u). \tag{1.12}$$

This model called $TV - L^2 - H^{-1}$, it contains the diffusion terms of $TV - L^2$ and $TV - H^{-1}$ model. However, it still suffers from the staircasing effect and the combination between the second and fourth-order diffusion terms leads to over-smooth homogeneous areas.

To overcome these limitations, we propose a nonlinear high order system, using the Weickert model [19], which is more efficient in reducing high noise intensity, combined with a decomposition suggested by Guo et al. [1] to control the diffusivity in smooth areas. This model corrects the disadvantages (staircasing phenomenon and over smoothing) of the diffusion term proposed in Eq (1.12).

(a) Noisy image **(b)** $TV - L^2 - H^{-1}$ **(c)** Proposed operator

Figure 1. First line: the restored image u, second line: its corresponding sharp edges for the real *Ice cream* image, contaminated by an unknown noise. We can observe that the staircasing effect is reduced using the Weickert operator during the denoising process, while tiny edges are well preserved.

We can see that in the Figure 1, where a denoising example is carried-out using the two diffusion operators. However, since the Weickert operator is strongly nonlinear, the computation of the solution using classical numerical approximation generates some blur effect. Hence, the introduction of the decomposition procedure, which will facilitate the treatment of the nonlinear part of the Weickert operator. However this decomposition is in general ill-posed and existence of the looked for solution is not ensured. In this work, we will check the existence and uniqueness of the solution in a suitable functional space inspired by the well-known Schauder fixed point theorem.

The organization of the main paper is given as follows. In section 2, we describe the new proposed model. Section 3 is devoted to the existence and uniqueness results of the solution to the proposed equation using Schauder fixed point theorem. After, we give a brief discretization part of the proposed coupled model PDE. At last, section 4 is devoted to numerical results and comparative experiments to improve our model.

2. Description of the proposed model

In this section, we have proposed a denoising model of non-variational type by modifying the diffusion term in Eq (1.12) to overcome its drawbacks. To take advantage of both the Perona-Malik model [20] and the Weickert model [19], we propose the new model given by the following equation:

$$\begin{cases} \frac{1}{2\lambda}\Big(div(D(J_\rho(\nabla u_\sigma))\nabla u)\Big) = \Delta^{-1}(f-u) \;\; in \;\; \Omega, \\ \langle D(J_\rho(\nabla u_\sigma))\nabla u, n\rangle = 0 \;\; on \;\; \partial\Omega, \end{cases} \tag{2.1}$$

where D is an anisotropic diffusion tensor and J_ρ is the structure tensor defined by

$$J_\rho(\nabla X_\sigma) = K_\rho * (\nabla X_\sigma \otimes \nabla X_\sigma). \tag{2.2}$$

where $*$ is the convolution product and $\otimes$ is the outer product defined such as $\nabla X_\sigma \otimes \nabla X_\sigma = \nabla X_\sigma (\nabla X_\sigma)^t$. Here X_σ is constructed using a convolution of X with a Gaussian kernel, while K_ρ and K_σ represent two Gaussian convolution kernels such as $K_\tau(x) = \frac{1}{2\pi\tau^2}\exp(-\frac{|x|^2}{2\tau^2})$. The function D is calculated using the tensor J_ρ eigenvalues and the eigenvectors as follows

$$D := \varphi_+(\upsilon_+, \upsilon_-)\theta_+\theta_+^T + \varphi_-(\upsilon_+, \upsilon_-)\theta_-\theta_-^T, \tag{2.3}$$

where $\upsilon_{+/-}$ and $\theta_{+/-}$ are respectively the eigenvalues and the eigenvectors of the tensor structure J_ρ, the eigenvalues $\upsilon_{+/-}$ are calculated as

$$\upsilon_{+/-} = \frac{1}{2}\left(trace(J_\rho) \pm \sqrt{trace^2(J_\rho) - 4\det(J_\rho)}\right). \tag{2.4}$$

While the functions φ_+ and φ_- represent the isotropic or anisotropic behavior of the smoothing on the image regions. Recently, an efficient choice of these functions is introduced in [21], where the authors consider the behavior of the Weickert model according to the two directions θ_+ and θ_-. The proposed coefficients take into account the diffusion in the vicinity of the contours and corners where the eigenvalues υ_+ and υ_- are very high. This choice is proposed as follows:

$$\begin{cases} \varphi_+(\upsilon_+, \upsilon_-) = \exp(-\frac{\upsilon_+}{k_1}), \\ \varphi_-(\upsilon_+, \upsilon_-) = \exp(-\frac{\upsilon_-}{k_2})(1 - \exp(-\frac{\upsilon_+}{k_1})), \end{cases} \tag{2.5}$$

where k_1 and k_2 are two thresholds defining the diffusion with respect to the directions θ_+ and θ_-, respectively.

Equation (2.1) is a highly nonlinear PDE and therefore its numerical solution is a non-trivial task. To overcome this difficulty, we follow the decomposition suggested in [1], introducing a splitting into the coupled system:

$$\begin{cases} div(D(J_\rho(\nabla u_\sigma))\nabla u) = \alpha v \quad in \quad \Omega, \\ \Delta v = f - u \quad in \quad \Omega, \\ \langle D(J_\rho(\nabla u_\sigma))\nabla u, n\rangle = \langle \nabla v, n\rangle = 0 \quad on \quad \partial\Omega, \end{cases} \tag{2.6}$$

Moreover, the solution (u, v) of system (2.6) is a stable state of the following evolutionary reaction-diffusion system

$$\begin{cases} \dfrac{\partial u}{\partial t} - div(D(J_\rho(\nabla u_\sigma))\nabla u) + \alpha v = 0 \quad in \quad \Omega \times (0, T), \\ \dfrac{\partial v}{\partial t} - \Delta v + f - u = 0 \quad in \quad \Omega \times (0, T), \\ \langle D(J_\rho(\nabla u_\sigma))\nabla u, n\rangle = \langle \nabla v, n\rangle = 0 \quad on \quad \partial\Omega \times (0, T), \\ u(x, 0) = f, \quad v(x, 0) = 0 \quad in \quad \Omega. \end{cases} \tag{2.7}$$

In order to establish the existence of the solution u associated to the problem (2.7), we introduce the following set of hypotheses (H) :

H_1 - The tensors D in $C^\infty(\mathbb{R}^{2\times2}, \mathbb{R}^{2\times2})$, positive-definite matrix and coercive with the coercivity constant is β.

H_2 - The initial condition f in $L^2(\Omega)$.

H_3 - The constants β, α, τ, ρ, σ, k_1 and k_2 are positives.

3. Existence and uniqueness

In this section, we give the variational formulation of the problem (2.7) and a priori estimations of the solution (u, v). Indeed, the variational formulation of the problem (2.7) is stated as follows

$$\begin{cases} \textit{Find } (u,v) \in (L^2(0,T;H^1(\Omega)))^2 \textit{and } (\frac{\partial u}{\partial t}, \frac{\partial v}{\partial t}) \in (L^2(0,T;H^1(\Omega)'))^2 \textit{ such that} \\ \begin{cases} \langle \frac{\partial u}{\partial t}, \phi \rangle + \int_\Omega D(J_\rho(\nabla u_\sigma))\nabla u \nabla \phi + \int_\Omega \alpha v \phi = 0, \\ \langle \frac{\partial v}{\partial t}, \phi \rangle + \int_\Omega \nabla v \nabla \phi + \int_\Omega f\phi - \int_\Omega u\phi = 0, \end{cases} \\ \forall \phi \in H^1(\Omega). \end{cases} \tag{3.1}$$

Inspired by the techniques employed by Catté et al. [22], for a nonlinear equation, we will show the existence result for our coupled problem of two equations. The following lemma gives some a priori estimations of the solution.

Lemma 1. *Assume that assumptions (H) are satisfied, then there exists a positive constant C, such that the weak solution of the problem (3.1) satisfies the following estimations*

$$\| u \|_{L^\infty(0,T;L^2(\Omega))} + \| u \|_{L^2(0,T;H^1(\Omega))} + \| \partial_t u \|_{L^2(0,T;H^1(\Omega)')} \leq C,$$

$$\| v \|_{L^\infty(0,T;L^2(\Omega))} + \| v \|_{L^2(0,T;H^1(\Omega))} + \| \partial_t v \|_{L^2(0,T;H^1(\Omega)')} \leq C,$$

Proof. We take $\phi = u$ in the first equation of (3.1) and $\phi = v$ in the second, we get

$$\begin{cases} \frac{d}{dt} \| u(t) \|^2_{L^2(\Omega)} + \int_\Omega D(J_\rho(\nabla u_\sigma))\nabla u \nabla u + \int_\Omega \alpha v u = 0, \\ \frac{d}{dt} \| v(t) \|^2_{L^2(\Omega)} + \int_\Omega \nabla v \nabla v + \int_\Omega f v - \int_\Omega u v = 0, \end{cases} \tag{3.2}$$

We integrate for $t \in (0, \tau]$ with $\tau \in (0, T]$, then we have

$$\begin{cases} \frac{1}{2} \| u(\tau) \|^2_{L^2(\Omega)} + \int_0^\tau \int_\Omega D(J_\rho(\nabla u_\sigma))\nabla u \nabla u + \int_0^\tau \int_\Omega \alpha v u = \frac{1}{2} \| u(0) \|^2_{L^2(\Omega)}, \\ \frac{1}{2} \| v(\tau) \|^2_{L^2(\Omega)} + \int_0^\tau \int_\Omega \nabla v \nabla v + \int_0^\tau \int_\Omega f v - \int_0^\tau \int_\Omega u v = \frac{1}{2} \| v(0) \|^2_{L^2(\Omega)}, \end{cases} \tag{3.3}$$

Multiplying the second equation of (3.3) by α and using the initial data $v(0) = 0$ and $u(0) = f$, then the equation becomes

$$\begin{cases} \frac{1}{2} \| u(\tau) \|^2_{L^2(\Omega)} + \int_0^\tau \int_\Omega D(J_\rho(\nabla u_\sigma))\nabla u \nabla u + \int_0^\tau \int_\Omega \alpha v u = \frac{1}{2} \| f \|^2_{L^2(\Omega)}, \\ \frac{\alpha}{2} \| v(\tau) \|^2_{L^2(\Omega)} + \alpha \int_0^\tau \int_\Omega \nabla v \nabla v + \alpha \int_0^\tau \int_\Omega f v - \alpha \int_0^\tau \int_\Omega u v = 0, \end{cases} \tag{3.4}$$

we add the two equations of (3.4), we get

$$\begin{aligned}\frac{1}{2} &\| u(\tau) \|^2_{L^2(\Omega)} + \frac{\alpha}{2} \| v(\tau) \|^2_{L^2(\Omega)} + \int_0^\tau \int_\Omega D(J_\rho(\nabla u_\sigma))\nabla u \nabla u \\ + &\alpha \int_0^\tau \int_\Omega \nabla v \nabla v + \int_0^\tau \int_\Omega \alpha f v = \frac{1}{2} \| f \|^2_{L^2(\Omega)}, \end{aligned} \tag{3.5}$$

On the one hand, applying Young's inequality we have

$$| \int_0^\tau \int_\Omega \alpha f v | \leq \frac{\alpha T}{2} \int_\Omega f^2 dx + \frac{\alpha}{2} \int_0^\tau \int_\Omega v^2 dx dt, \tag{3.6}$$

On the other hand, thanks to the coercivity of D, we see that

$$\int_0^\tau \int_\Omega D(J_\rho(\nabla u_\sigma))\nabla u \nabla u \geq \beta \int_0^\tau \int_\Omega \nabla u \nabla u \tag{3.7}$$

Using (3.7) and (3.6), Eq (3.5) becomes

$$\frac{1}{2} \| u(\tau) \|^2_{L^2(\Omega)} + \frac{\alpha}{2} \| v(\tau) \|^2_{L^2(\Omega)} + \beta \int_0^\tau \int_\Omega \nabla u \nabla u + \alpha \int_0^\tau \int_\Omega \nabla v \nabla v \tag{3.8}$$

$$\leq \frac{\alpha T + 1}{2} \int_\Omega f^2 dx + \frac{\alpha}{2} \int_0^\tau \int_\Omega v^2 dx dt, \tag{3.9}$$

Setting $K(\tau) = \int_\Omega v(\tau)^2$, we see that

$$K(\tau) \leq \frac{\alpha T + 1}{\alpha} \int_\Omega f^2 dx + \int_0^\tau K(t).$$

Using the Gronwall's inequality, we get

$$K(\tau) \leq \frac{\alpha T + 1}{\alpha} \| f \|^2_{L^2(\Omega)} \exp(\tau),$$

which implies that

$$\int_\Omega v(\tau)^2 \leq C$$

where the constant depends on T, we deduce that v is bounded in $L^\infty(0, T; L^2(\Omega))$. Hence

$$\| u \|_{L^\infty(0,T;L^2(\Omega))} + \| v \|_{L^\infty(0,T;L^2(\Omega))} + \beta \int_0^\tau \int_\Omega \nabla u \nabla u + \alpha \int_0^\tau \int_\Omega \nabla v \nabla v \leq C.$$

By taking Eq (3.8) and by adding the term $\beta \int_0^\tau \int_\Omega u^2 + \alpha \int_0^\tau \int_\Omega v^2$ to both sides we get

$$\frac{1}{2} \| u(\tau) \|^2_{L^2(\Omega)} + \frac{\alpha}{2} \| v(\tau) \|^2_{L^2(\Omega)} + \beta(\int_0^\tau \int_\Omega \nabla u \nabla u + u^2) + \alpha(\int_0^\tau \int_\Omega \nabla v \nabla v + v^2)$$

$$\leq \frac{\alpha T+1}{2}\int_\Omega f^2dx+\frac{3\alpha}{2}\int_0^\tau\int_\Omega v^2dxdt+\int_0^\tau\int_\Omega u^2dxdt,$$

which means that:

$$\begin{cases}\| u \|_{L^\infty(0,T;L^2(\Omega))}\leq C,\\ \| u \|_{L^2(0,T;H^1(\Omega))}\leq C,\\ \| v \|_{L^\infty(0,T;L^2(\Omega))}\leq C,\\ \| v \|_{L^2(0,T;H^1(\Omega))}\leq C.\end{cases} \tag{3.10}$$

Let's prove now the estimation of $\frac{\partial u}{\partial t}$ and $\frac{\partial v}{\partial t}$. For that, let's back to Eq (3.1), we have for all ϕ

$$\begin{cases}|\langle\frac{\partial u}{\partial t},\phi\rangle|=|\int_\Omega D(J_\rho(\nabla u_\sigma))\nabla u\nabla\phi-\int_\Omega\alpha v\phi|,\\ |\langle\frac{\partial v}{\partial t},\phi\rangle|=|\int_\Omega\nabla v\nabla\phi-\int_\Omega f\phi+\int_\Omega u\phi|,\end{cases} \tag{3.11}$$

using hypotheses H_1 and Hölder inequality we get

$$\begin{cases}|\langle\frac{\partial u}{\partial t},\phi\rangle|\leq\| D(J_\rho(\nabla u_\sigma))\|_{L^\infty(\Omega)}\|\nabla u\|_{L^2(\Omega)}\|\nabla\phi\|_{L^2(\Omega)}+\alpha\|v\|_{L^2(\Omega)}\|\phi\|_{L^2(\Omega)},\\ |\langle\frac{\partial v}{\partial t},\phi\rangle|\leq\|\nabla v\|_{L^2(\Omega)}\|\nabla\phi\|_{L^2(\Omega)}+\|f\|_{L^2(\Omega)}\|\phi\|_{L^2(\Omega)}+\|u\|_{L^2(\Omega)}\|\phi\|_{L^2(\Omega)},\end{cases} \tag{3.12}$$

or $\|\nabla\phi\|_{L^2(\Omega)}\leq\|\phi\|_{H^1(\Omega)}$ and $\|\phi\|_{L^2(\Omega)}\leq\|\phi\|_{H^1(\Omega)}$, then the previous equation becomes

$$\begin{cases}|\langle\frac{\partial u}{\partial t},\phi\rangle|\leq\| D(J_\rho(\nabla u_\sigma))\|_{L^\infty(\Omega)}\|\nabla u\|_{L^2(\Omega)}\|\phi\|_{H^1(\Omega)}+\alpha\|v\|_{L^2(\Omega)}\|\phi\|_{H^1(\Omega)},\\ |\langle\frac{\partial v}{\partial t},\phi\rangle|\leq\|\nabla v\|_{L^2(\Omega)}\|\phi\|_{H^1(\Omega)}+\|f\|_{L^2(\Omega)}\|\phi\|_{H^1(\Omega)}+\|u\|_{L^2(\Omega)}\|\phi\|_{H^1(\Omega)},\end{cases} \tag{3.13}$$

this means

$$\begin{cases}\|\frac{\partial u}{\partial t}\|_{(H^1(\Omega))'}\leq\| D(J_\rho(\nabla u_\sigma))\|_{L^\infty(\Omega)}\|\nabla u\|_{L^2(\Omega)}+\alpha\|v\|_{L^2(\Omega)},\\ \|\frac{\partial v}{\partial t}\|_{(H^1(\Omega))'}\leq\|\nabla v\|_{L^2(\Omega)}+\|f\|_{L^2(\Omega)}+\|u\|_{L^2(\Omega)},\end{cases} \tag{3.14}$$

integrating over $t\in(0,T]$, we find

$$\begin{cases}\|\frac{\partial u}{\partial t}\|_{L^2(0,T;H^1(\Omega)')}\leq\| D(J_\rho(\nabla u_\sigma))\|_{L^\infty(0,T;L^\infty(\Omega))}\|\nabla u\|_{L^2(0,T;L^2(\Omega))}+\alpha\|v\|_{L^2(0,T;L^2(\Omega))},\\ \|\frac{\partial v}{\partial t}\|_{L^2(0,T;H^1(\Omega)')}\leq\|\nabla v\|_{L^2(0,T;L^2(\Omega))}+T\|f\|_{L^2(\Omega)}+\|u\|_{L^2(0,T;L^2(\Omega))},\end{cases} \tag{3.15}$$

and according to estimates in (11), we conclude that

$$\begin{cases}\|\frac{\partial u}{\partial t}\|_{L^2(0,T;H^1(\Omega)')}\leq C,\\ \|\frac{\partial v}{\partial t}\|_{L^2(0,T;H^1(\Omega)')}\leq C.\end{cases} \tag{3.16}$$

which ends the proof. □

The following theorem shows the existence and uniqueness of a solution to the proposed model

Theorem 1. *Let $f\in L^2(\Omega)$ and $T>0$, under the assumptions above, the problem (2.7) admits a unique weak solution $(u,v)\in C(0,T;L^2(\Omega))\cap L^2(0,T;H^1(\Omega))$.*

3.1. Existence

For the proof of existence, we use the classical Schauder fixed point theorem [23, theorem 2.A, p. 56]. To define the fixed point operator, we introduce first these spaces

$$V(0,T) = \left\{ w \in L^2(0,T;H^1(\Omega)),\ \partial_t w \in L^2(0,T;H^1(\Omega)^{'}) \right\}$$

which is a Hilbert space equipped with the norm

$$\| w \|_{V(0,T)} = \| w \|_{L^2(0,T;H^1(\Omega))} + \| \partial_t w \|_{L^2(0,T;H^1(\Omega)')}$$

and

$$V_0 = \Big\{ w \in V(0,T) : \| w \|_{L^\infty(0,T;L^2(\Omega))} \leq C,\ \| w \|_{L^2(0,T;H^1(\Omega))} \leq C,$$
$$\| \partial_t w \|_{L^2(0,T;H^1(\Omega)'))} \leq C, \text{ and } w(0) = f \Big\}$$

which is a nonempty, convex and weakly compact subset of $V(0,T)$. The estimations introduced in the functional space V_0 are deduced from the precedent lemma 1.
The Schauder's fixed point operator is given as follows

$$\begin{aligned} L \ &: \ V_0 \ \rightarrow \ V_0 \\ &w \mapsto L(w) = u_w \end{aligned}$$

where u_w is the solution associated to (w, v) for the following problem

$$\begin{cases} \langle \dfrac{\partial u}{\partial t}, \phi \rangle + \displaystyle\int_\Omega D(J_\rho(\nabla w_\sigma))\nabla u \nabla \phi + \int_\Omega \alpha v \phi = 0, \\ \langle \dfrac{\partial v}{\partial t}, \psi \rangle + \displaystyle\int_\Omega \nabla v \nabla \psi + \int_\Omega f\psi - \int_\Omega u\psi = 0, \\ \forall \phi, \psi \in (H^1(\Omega))^2, \\ u(0) = f \text{ and } v(0) = 0. \end{cases} \tag{3.17}$$

which is now linear in u. As a result and using the theoretical existence of parabolic equations results [24, Theorem 3, p. 356], we ensure that the problem (3.17) has a unique solution (u_w, v) in $V(0,T)$.
The existence of a weak solution for the problem (3.1) is equivalent to the existence of a fixed point for the operator L. For this reason, we apply Schauder's fixed point theorem, which requires only to prove that the mapping L is weakly continuous. For that, let $(w_n)_{n\in\mathbb{N}}$ be a sequence in V_0 such that $w_n \rightharpoonup w$ in V_0, and $u_n = L(w_n)$, we should prove that

$$u_n = L(w_n) \rightharpoonup u_w = L(w) \text{ in } V_0.$$

Using the compact inclusions of Sobolev spaces [25] and by estimations established in lemma 1, there exists a subsequence noted also $(w_n, v_n)_{n\in\mathbb{N}}$ and (u_n, v_n) such that

$$\begin{cases} \dfrac{\partial u_n}{\partial t} \rightharpoonup \dfrac{\partial u}{\partial t} \text{ and } \dfrac{\partial v_n}{\partial t} \rightharpoonup \dfrac{\partial v}{\partial t} & \text{in } L^2(0,T;H^1(\Omega)^{'}) \\ u_n \rightarrow u \text{ and } v_n \rightarrow v & \text{in } L^2(0,T;L^2(\Omega)) \\ \nabla u_n \rightharpoonup \nabla u \text{ and } \nabla v_n \rightharpoonup \nabla v & \text{in } (L^2(0,T;L^2(\Omega)))^2 \\ w_n \rightarrow w & \text{in } L^2(0,T;L^2(\Omega)) \\ D(J_\rho(\nabla w_{n\sigma})) \rightarrow D(J_\rho(\nabla w_\sigma)) & \text{in } L^2(0,T;L^2(\Omega)) \\ u_n(0) \rightarrow u(0) & \text{in } H^1(\Omega)^{'} \end{cases} \tag{3.18}$$

Using these convergences and by the uniqueness of the solution of (3.17), we have

$$u_n = L(w_n) \rightharpoonup u = L(w) \text{ in } V_0.$$

This proves that L is weakly continuous. Finally from the Schauder fixed point theorem, the operator L admits a fixed point solution to the problem (3.1). Moreover, since $u, v \in L^2(0,T;H^1(\Omega))$ and $\frac{\partial u}{\partial t}, \frac{\partial v}{\partial t} \in L^2(0,T;H^1(\Omega)')$, by Aubin's theorem [26], we deduce that $u, v \in C(0,T;L^2(\Omega))$.

3.2. Uniqueness

In order to show that the solution of (2.7) is unique, we consider two different solutions (u_1, v_1) and (u_2, v_2) to the problem (2.7). Then we have

$$\begin{cases} \langle \frac{\partial u_1}{\partial t}, \phi \rangle + \int_\Omega D(J_\rho(\nabla u_{1\sigma}))\nabla u_1 \nabla \phi + \int_\Omega \alpha v_1 \phi = 0, \\ \langle \frac{\partial v_1}{\partial t}, \phi \rangle + \int_\Omega \nabla v_1 \nabla \phi + \int_\Omega f\phi - \int_\Omega u_1 \phi = 0, \end{cases} \tag{3.19}$$

and

$$\begin{cases} \langle \frac{\partial u_2}{\partial t}, \phi \rangle + \int_\Omega D(J_\rho(\nabla u_{2\sigma}))\nabla u_2 \nabla \phi + \int_\Omega \alpha v_2 \phi = 0, \\ \langle \frac{\partial v_2}{\partial t}, \phi \rangle + \int_\Omega \nabla v_2 \nabla \phi + \int_\Omega f\phi - \int_\Omega u_2 \phi = 0, \end{cases} \tag{3.20}$$

By subtracting both variational formulation of (u_1, v_1) and (u_2, v_2), we obtain

$$\begin{cases} \langle \frac{\partial (u_1 - u_2)}{\partial t}, \phi \rangle + \int_\Omega (D(J_\rho(\nabla u_{1\sigma}))\nabla u_1 - D(J_\rho(\nabla u_{2\sigma}))\nabla u_2)\nabla \phi + \int_\Omega \alpha(v_1 - v_2)\phi = 0, \\ \langle \frac{\partial (v_1 - v_2)}{\partial t}, \phi \rangle + \int_\Omega \nabla(v_1 - v_2)\nabla \phi - \int_\Omega (u_1 - u_2)\phi = 0, \end{cases} \tag{3.21}$$

We take $\phi = u_1 - u_2$ in the first equation of (3.21) and $\phi = v_1 - v_2$ in the second, we get

$$\begin{cases} \frac{d}{2dt} \| u_1(t) - u_2(t) \|^2_{L^2(\Omega)} + \int_\Omega (D(J_\rho(\nabla u_{1\sigma}))(\nabla(u_1(t) - u_2(t)))^2 \\ + \int_\Omega (D(J_\rho(\nabla u_{1\sigma})) - D(J_\rho(\nabla u_{2\sigma})))\nabla u_2 \nabla(u_1(t) - u_2(t)) + \int_\Omega \alpha(v_1 - v_2)(u_1 - u_2) = 0, \\ \frac{d}{2dt} \| v_1(t) - v_2(t) \|^2_{L^2(\Omega)} + \int_\Omega (\nabla(v_1 - v_2))^2 - \int_\Omega (u_1 - u_2)(v_1 - v_2) = 0, \end{cases} \tag{3.22}$$

Now, multiplying the second equation of (3.22) by α and adding the two equations we get

$$\begin{aligned} &\frac{d}{2dt} \| u_1(t) - u_2(t) \|^2_{L^2(\Omega)} + \alpha \frac{d}{2dt} \| v_1(t) - v_2(t) \|^2_{L^2(\Omega)} + \int_\Omega (D(J_\rho(\nabla u_{1\sigma}))(\nabla(u_1(t) - u_2(t)))^2 \\ &+ \int_\Omega (D(J_\rho(\nabla u_{1\sigma})) - D(J_\rho(\nabla u_{2\sigma})))\nabla u_2 \nabla(u_1(t) - u_2(t)) + \alpha \int_\Omega (\nabla(v_1 - v_2))^2 = 0 \end{aligned}$$

Thanks to the coercivity of D, we have

$$\frac{d}{2dt} \| u_1(t) - u_2(t) \|^2_{L^2(\Omega)} + \alpha \frac{d}{2dt} \| v_1(t) - v_2(t) \|^2_{L^2(\Omega)} + \beta \| \nabla(u_1(t) - u_2(t)) \|^2_{L^2(\Omega)}$$

$$+\alpha \parallel \nabla(v_1(t)-v_2(t)) \parallel^2_{L^2(\Omega)} \leq \parallel D(J_\rho(\nabla u_{1\sigma})) - D(J_\rho(\nabla u_{2\sigma})) \parallel_{L^\infty(\Omega)} \int_\Omega \mid \nabla u_2(t) \mid \mid \nabla(u_1(t)-u_2(t)) \mid$$

Since the operator $D(J_\rho)$ is smooth enough, we have

$$\parallel D(J_\rho(\nabla u_{1\sigma})) - D(J_\rho(\nabla u_{2\sigma})) \parallel_{L^\infty(\Omega)} \leq c \parallel u_1(t)-u_2(t) \parallel_{L^2(\Omega)} \tag{3.23}$$

Using (3.23) and hypothesis (H_1), and Holder inequality, we have

$$\frac{d}{2dt} \parallel u_1(t)-u_2(t) \parallel^2_{L^2(\Omega)} + \alpha \frac{d}{2dt} \parallel v_1(t)-v_2(t) \parallel^2_{L^2(\Omega)} + \beta \parallel \nabla(u_1(t)-u_2(t)) \parallel^2_{L^2(\Omega)}$$

$$+\alpha \parallel \nabla(v_1(t)-v_2(t)) \parallel^2_{L^2(\Omega)} \leq c \parallel u_1(t)-u(t) \parallel_{L^2(\Omega)} \parallel \nabla u_2(t) \parallel_{L^2(\Omega)} \parallel \nabla(u_1(t)-u_2(t)) \parallel_{L^2(\Omega)}$$

Integrating over $[0, s)$ with $s \in (0, T]$ and applying Young's inequality for enough epsilon, we have

$$\frac{1}{2} \parallel u_1(s)-u_2(s) \parallel^2_{L^2(\Omega)} + (\beta - \frac{\varepsilon}{2}) \int_0^s \parallel \nabla(u_1(t)-u_2(t)) \parallel^2_{L^2(\Omega)} dt$$

$$\leq \frac{c}{2\varepsilon} \int_0^s \parallel u_1(t)-u_2(t) \parallel^2_{L^2(\Omega)} \parallel \nabla u_2(t) \parallel^2_{L^2(\Omega)} dt$$

For $\varepsilon < 2\beta$, we have

$$\frac{1}{2} \parallel u_1(s)-u_2(s) \parallel^2_{L^2(\Omega)} \leq \frac{c}{2\varepsilon} \int_0^s \parallel u_1(t)-u_2(t) \parallel^2_{L^2(\Omega)} \parallel \nabla u_2(t) \parallel^2_{L^2(\Omega)} dt.$$

Using Gronwall's inequality we have

$$u_1 = u_2.$$

Now back to the second equation of (3.22), we have

$$\frac{d}{2dt} \parallel v_1(t)-v_2(t) \parallel^2_{L^2(\Omega)} + \int_\Omega (\nabla(v_1-v_2))^2 = 0$$

which means that $v_1 = v_2$,
Hence

$$(u_1, v_1) = (u_2, v_2).$$

4. Discrete setting

In this section, we are interested in the numerical approximation of the proposed model. In fact, to compute numerically the problem (2.7), we carry out a fully discretization of the model using finite difference method.
Assume k to be the time step size and h the spatial grid size, we discretize time and space as follows:

$$\begin{aligned} t_n &= nk, \quad n = 0, 1, 2...., \\ x_i &= ih, \quad i = 0, 1, 2, ..., M, \\ y_j &= jh, \quad j = 0, 1, 2, ..., N. \end{aligned}$$

Denote $u^n_{i,j}$, $v^n_{i,j}$ and $f_{i,j}$ the approximations of $u(t_n, x_i, y_j)$, $v(t_n, x_i, y_j)$ and $f(x, y)$ respectively, then we

define the discrete approximations :

$$\frac{\partial u(t,x,y)}{\partial t} = \frac{u_{i,j}^{n+1} - u_{i,j}^{n}}{k} \text{ and } \frac{\partial v(t,x,y)}{\partial t} = \frac{v_{i,j}^{n+1} - v_{i,j}^{n}}{k}$$
$$\Delta v_{i,j}^{n} = \frac{v_{i,j-1}^{n} + v_{i,j+1}^{n} - 4v_{i,j}^{n} + v_{i-1,j}^{n} + v_{i+1,j}^{n}}{h^2}$$

it remains now to discretize the term of diffusion $div(D(J_\rho(\nabla u_\sigma))\nabla u)$, to do so, we consider the method represented by Weickert [19, Chapter 3], which consists of acting by convolution on the discrete image in any pixel with kernel, called a non-negative stencil. For that we write the diffusion tensor such as $\begin{pmatrix} a & b \\ b & c \end{pmatrix}$ which is calculated by the structure tensor $J_\rho(\nabla u_\sigma)$, then the term of diffusion can be rewritten as

$$div(D(J_\rho(\nabla u_\sigma))\nabla u) = div[\begin{pmatrix} a & b \\ b & c \end{pmatrix}\begin{pmatrix} \partial_x u \\ \partial_y u \end{pmatrix}] = \partial_x(a\partial_x(u)) + \partial_x(b\partial_y(u)) + \partial_y(b\partial_x(u)) + \partial_y(c\partial_y(u)) \tag{4.1}$$

Hence, the discretization of the diffusion term is given by

$$\begin{aligned}[div(D(J_\rho(\nabla u_\sigma))\nabla u^n)]_{i,j} = (\partial_x a)_{i,j}(\partial_x u^n)_{i,j} + a_{i,j}(\partial_{xx} u^n)_{i,j} + (\partial_x b)_{i,j}(\partial_y u^n)_{i,j} + b_{i,j}(\partial_{xy} u^n)_{i,j} \\ +(\partial_y b)_{i,j}(\partial_x u^n)_{i,j} + b_{i,j}(\partial_{yx} u^n)_{i,j} + (\partial_y c)_{i,j}(\partial_y u^n)_{i,j} + c_{i,j}(\partial_{yy} u^n)_{i,j}\end{aligned} \tag{4.2}$$

then this standard discretization is equivalent to acting by convolution on the image u at any point (i, j) by a matrix of size 3×3 called by the Stencil matrix denoted by S [19, Chapter 3,p. 95], if $A(u)$ indicates the matrix containing the elements of term $div(D(J_\rho(\nabla u_\sigma))\nabla u)$ after the discretization, then an element of $A(u)$ is calculated by

$$\begin{aligned}[A(u^n)]_{i,j} = u_{i-1,j-1}^{n} s_{11} + u_{i-1,j}^{n} s_{12} + u_{i-1,j+1}^{n} s_{13} + u_{i,j-1}^{n} s_{21} \\ +u_{i,j}^{n} s_{22} + u_{i,j+1}^{n} s_{23} + u_{i+1,j-1}^{n} s_{31} + u_{i+1,j}^{n} s_{32} + u_{i+1,j+1}^{n} s_{33}\end{aligned}$$

Finally, the discrete explicit scheme of the problem (2.7) could be written as

$$\begin{cases} u_{i,j}^{n+1} = u_{i,j}^{n} + k([A(u^n)]_{i,j} - \alpha v_{i,j}^{n}), \\ v_{i,j}^{n+1} = v_{i,j}^{n} + k(\Delta v_{i,j}^{n} - f_{i,j} + u_{i,j}^{n}), \\ u_{i,j}^{0} = f_{i,j}, \ v_{i,j}^{0} = 0. \end{cases} \tag{4.3}$$

for all $k \geq 0$, $0 \leq i \leq N$ and $0 \leq j \leq M$.

5. Numerical results

In this section, we illustrate the performance of the proposed model for image denoising. For a fair comparison, these methods are implemented using Matlab 2012a on the platform: 3 GHz dual-core CPU and 8 Gbytes RAM. We use the relative error (E_r) as a stopping criteria of the following numerical simulations, which is defined by

$$E_r = \frac{\|u^{n+1} - u^n\|_{L^2}}{\|u^n\|_{L^2}} < 10^{-5},$$

where u^n is the restored image at the iteration n.

We have tested the proposed multi-frame SR method on a large database image using different applications, we present in the following experiments only some of them. Two commonly used quality measures are considered to evaluate the denoising performance, i.e., PSNR and the SSIM indexes. For the following tests we fix the parameters of our method such as $k = 0.15$, $\alpha = 0.01$, $\rho = 1.4$ $\sigma = 1.6$ and $maxIter = 500$. While the values of k_1 and k_2 are chosen with respect to the best PSNR values. For the following tests, we chose $k_1 \in [30, 150]$ and $k_2 \in [10, 250]$, respectively.

In order to validate our model in computing the component u and v, we begin with validation tests, where we select four noisy images (with different standard deviation σ). In Figure 2, we have presented the restored image u and the computed component v for each test. From this figure it is clear that our model is able to recover image features even if the noise level is high.

For a convenient comparison, we compare our method with some competitive denoising methods, among them: the TV-H^{-1} [13], the telegraph coupled partial differential equation (TCPDE) proposed in [27], TV-L^2-H^{-1} [17], the fourth-order PDE (FOPDE) [28] and also the nonlinear fractional reaction-diffusion system (NFAD) [15]. Note that concerning the chosen parameters for the proposed algorithm, we take $k_1 = 55$, $k_2 = 45$, $k = 0.1$, $\alpha = 0.01$, $\rho = 3.2$, time step size $k = 0.1$, $\sigma = 2.2$ and $maxIter = 1000$. In contrast, the used parameters for the compared methods are chosen inspired from the given parameters in numerical results of their respective papers. In fact, the used parameters for these methods (including the proposed one) corresponding to the following tests are depicted in Table 1.

Table 1. The set of parameters being used in denoising results presented in the three following tests.

Parameters	Method					
	FOPDE	TV-H^{-1}	TV-L^2-H^{-1}	TCPDE	NFAD	Our Method
Iteration number N	1000	1000	1000	1000	1000	1000
The time step size Δt	0.1	0.001	1	0.1	—	0.1
The parameter α_1	0.06	—	—	0.02	0.065	—
Spatially decaying effect (k_1, k_2)	$(100, 44)$	—	—	—	—	$(35, 35)$
The fractional order derivative β	—	—	—	—	1.77	—
Regularization parameter η	—	0.01	0.01	0.01	—	—
The parameter λ	—	1	10	—	—	—

- Firstly, we consider the "*Motif*" image and we configure a simulated test. We add a Gaussian noise with parameter $\sigma = 30$. The restored images using different denoising approaches are shown in Figure 3 and the associated 3D surfaces in Figure 4. We can see that the proposed reaction-diffusion equation outperforms the other methods and we can see the difference better in the smooth areas, where the staircasing effect is efficiently avoided.

- The next experiments deals with *Drop* image, which is contaminated by a Gaussian noise with standard deviation $\sigma = 40$. The aim is to restore the clean image and compare it with the other denoising methods. The obtained results for the three tests are shown in Figure 5. As the previous test, the proposed PDE-constrained equation gives the better result. We can see the difference better in the 3D plots, where we show the image region surfaces of each restored image in Figure 6. As a result, it is quite visible that the proposed method demonstrates clearly it performance

as seen in the restored image: edges are efficiently preserved, homogeneous areas are free from noise and low-contrast objects are quite visible. This conforms the fact, that the idea of computing the couple u and v with the tensor diffusion deals with the competitive image denoising techniques.

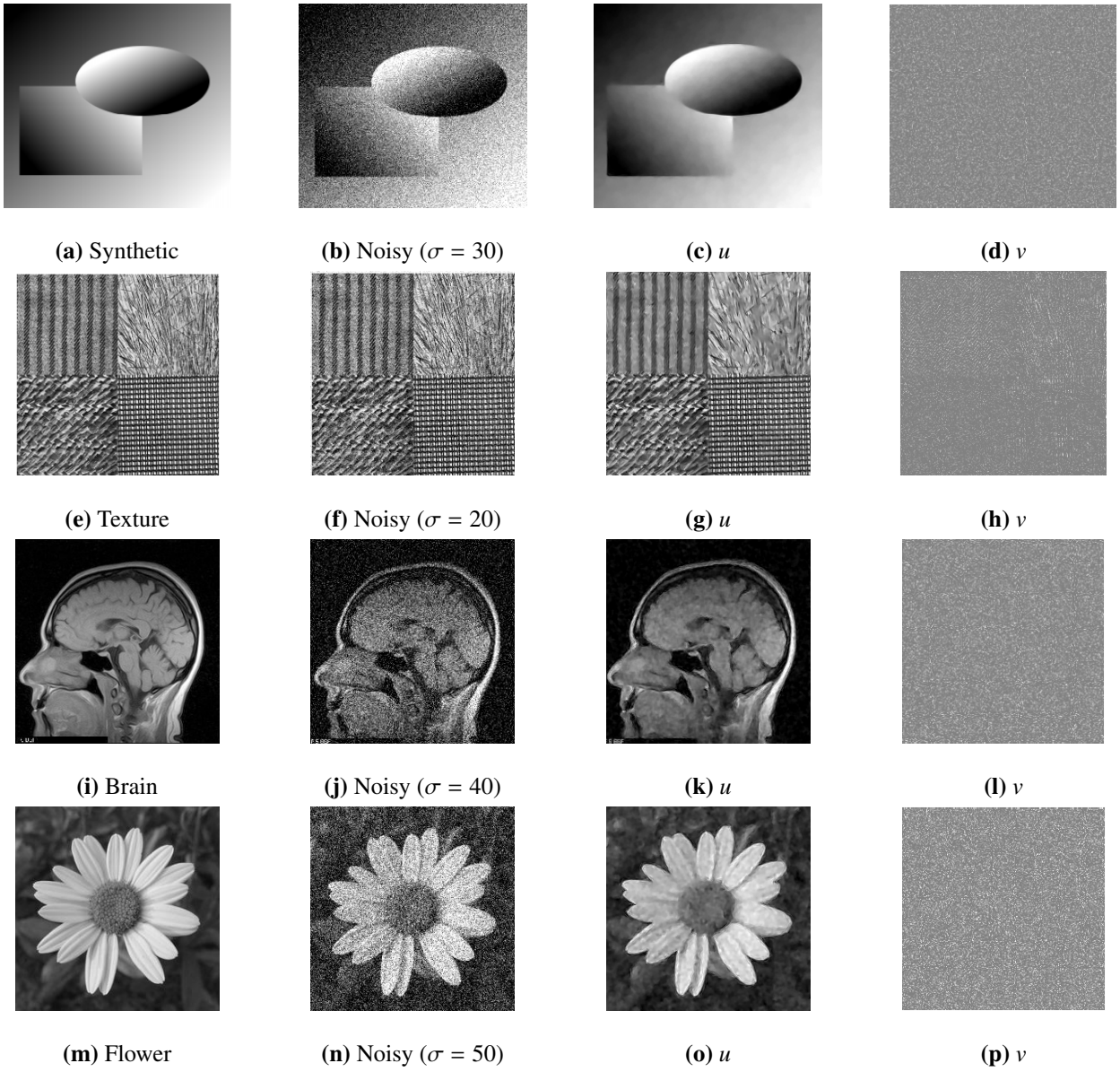

(a) Synthetic **(b)** Noisy (σ = 30) **(c)** u **(d)** v

(e) Texture **(f)** Noisy (σ = 20) **(g)** u **(h)** v

(i) Brain **(j)** Noisy (σ = 40) **(k)** u **(l)** v

(m) Flower **(n)** Noisy (σ = 50) **(o)** u **(p)** v

Figure 2. The restored image u, its corresponding v for the four images with different Gaussian noise levels.

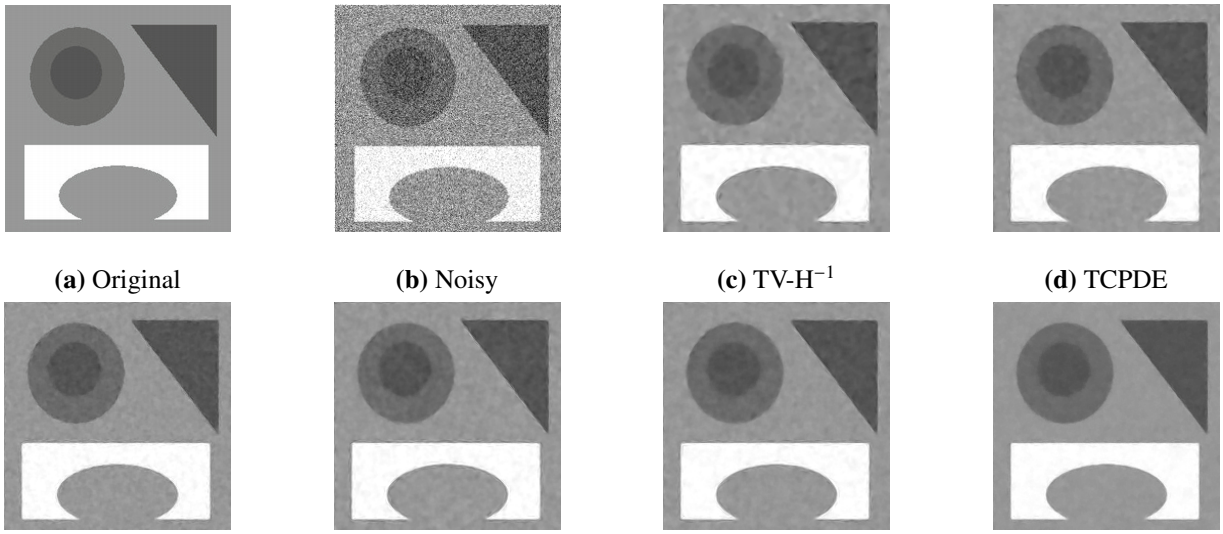

(a) Original **(b)** Noisy **(c)** TV-H^{-1} **(d)** TCPDE

(e) TV-L^2-H^{-1} **(f)** FOPDE **(g)** NFAD **(h)** Our

Figure 3. *Motif* image corrupted by Gaussian noise with $\sigma = 55$ and restored by different denoising models.

- For the third test we use *Brain* image, we added a Gaussian noise with $\sigma = 50$. In Figure 7, we present the restored image using different enhancement methods. Once again, we can see clearly the robustness of the proposed PDE compared with the other ones. This also confirmed in Figure 10, where we present the respective 3D surfaces. A we can see the image regions recovered by our method look very close to the ones of the original image, which is not the case of the compared methods.

To give a fair and quantitative comparison with the other methods, we use the PSNR and SSIM measures. Effectively, we show the evolution of the PSNR and SSIM with respect to the first 1000 iterations for the proposed and compared methods in Figure 9. We can see once again that always our approach reaches the best PSNR and SSIM values for the three tests.

Finally, we propose two real MRI tests downloaded from*, where the images are corrupted by unknown noise supposed to be of Poisson type. The aim is to recover a clean image with strong edges and considerable contrast. Figure 10 illustrated the recovered *MRI Head* using different denoising approaches, while Figure 11 presents the obtained clean image u for the real *MRI Knee* image with comparison to other methods. The final two results obtained using the proposed equation clearly indicates that the significant edges and textures are recovered with less blurring and staircasing. As a conclusion, from these real images, it is easy to observe that the proposed PDE is more efficient to remove almost all noise particles with effective structure preservation without information about the noise type.

*www.mr-tip.com

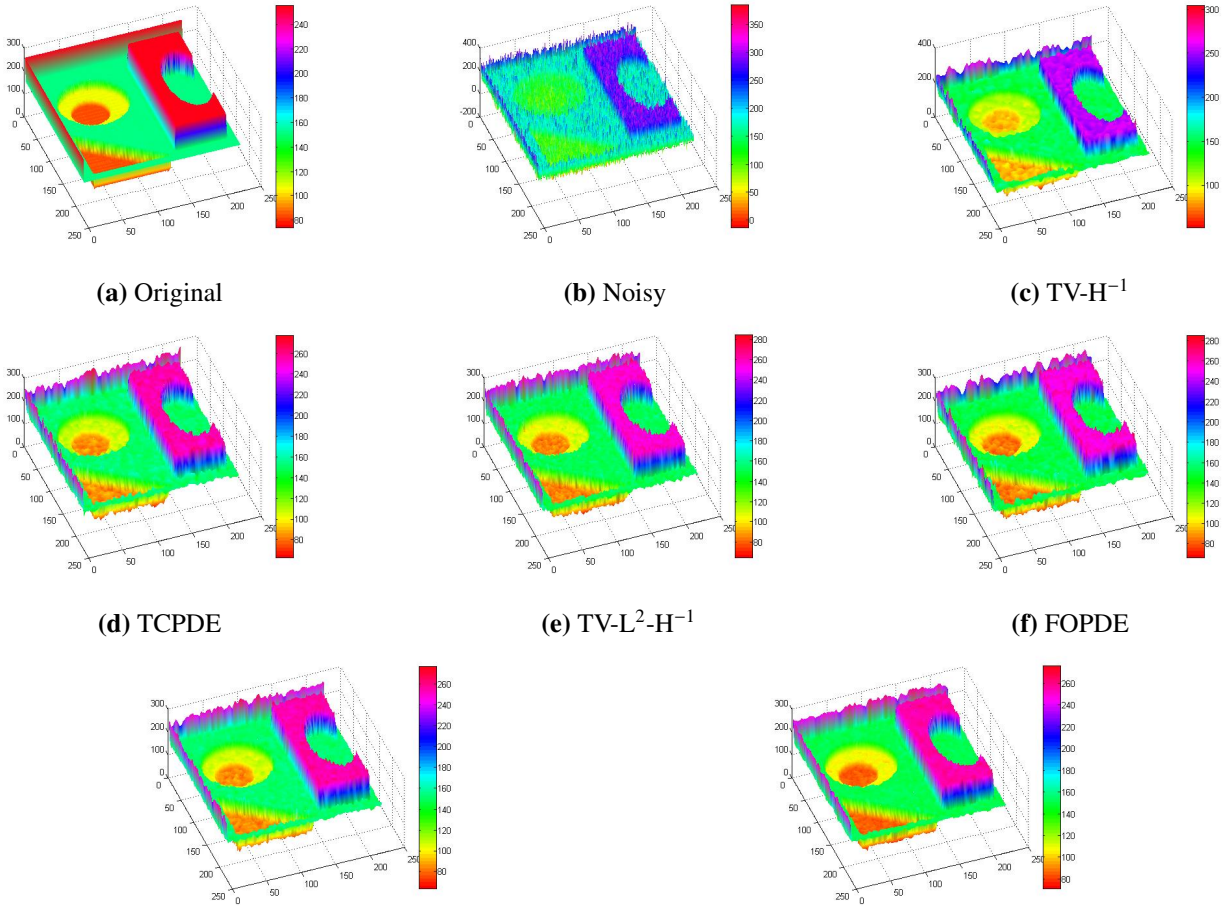

(a) Original **(b)** Noisy **(c)** TV-H^{-1}

(d) TCPDE **(e)** TV-L^2-H^{-1} **(f)** FOPDE

(g) NFAD **(h)** Our

Figure 4. The 3D surface representations of the recovered images in Figure 3.

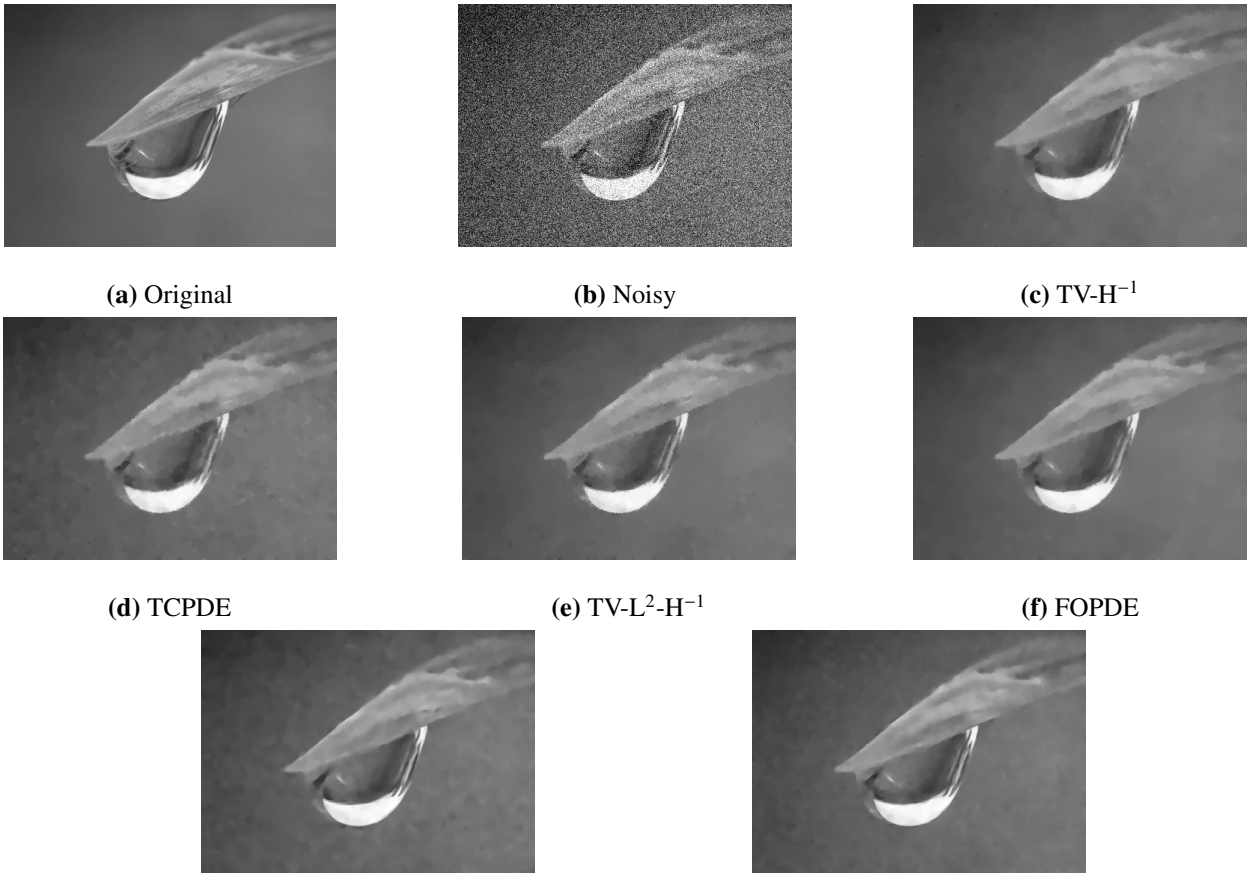

(a) Original **(b)** Noisy **(c)** TV-H^{-1}

(d) TCPDE **(e)** TV-L^2-H^{-1} **(f)** FOPDE

(g) NFAD **(h)** Our

Figure 5. *Drop* image corrupted by Gaussian noise with $\sigma = 40$ and restored by different denoising models.

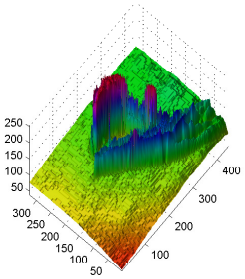

(a) Original

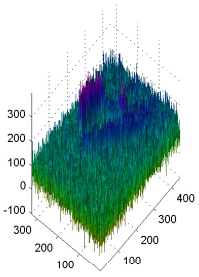

(b) Noisy

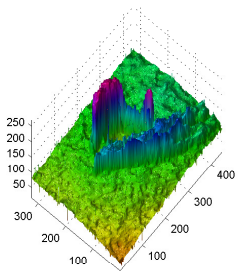

(c) TV-H^{-1}

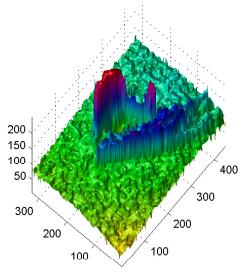

(d) TCPDE

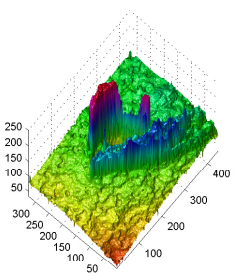

(e) TV-L^2-H^{-1}

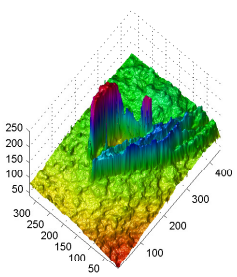

(f) FOPDE

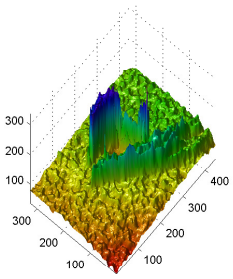

(g) NFAD

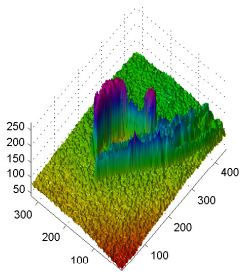

(h) Our

Figure 6. The 3D surface representations of the recovered images in Figure 5.

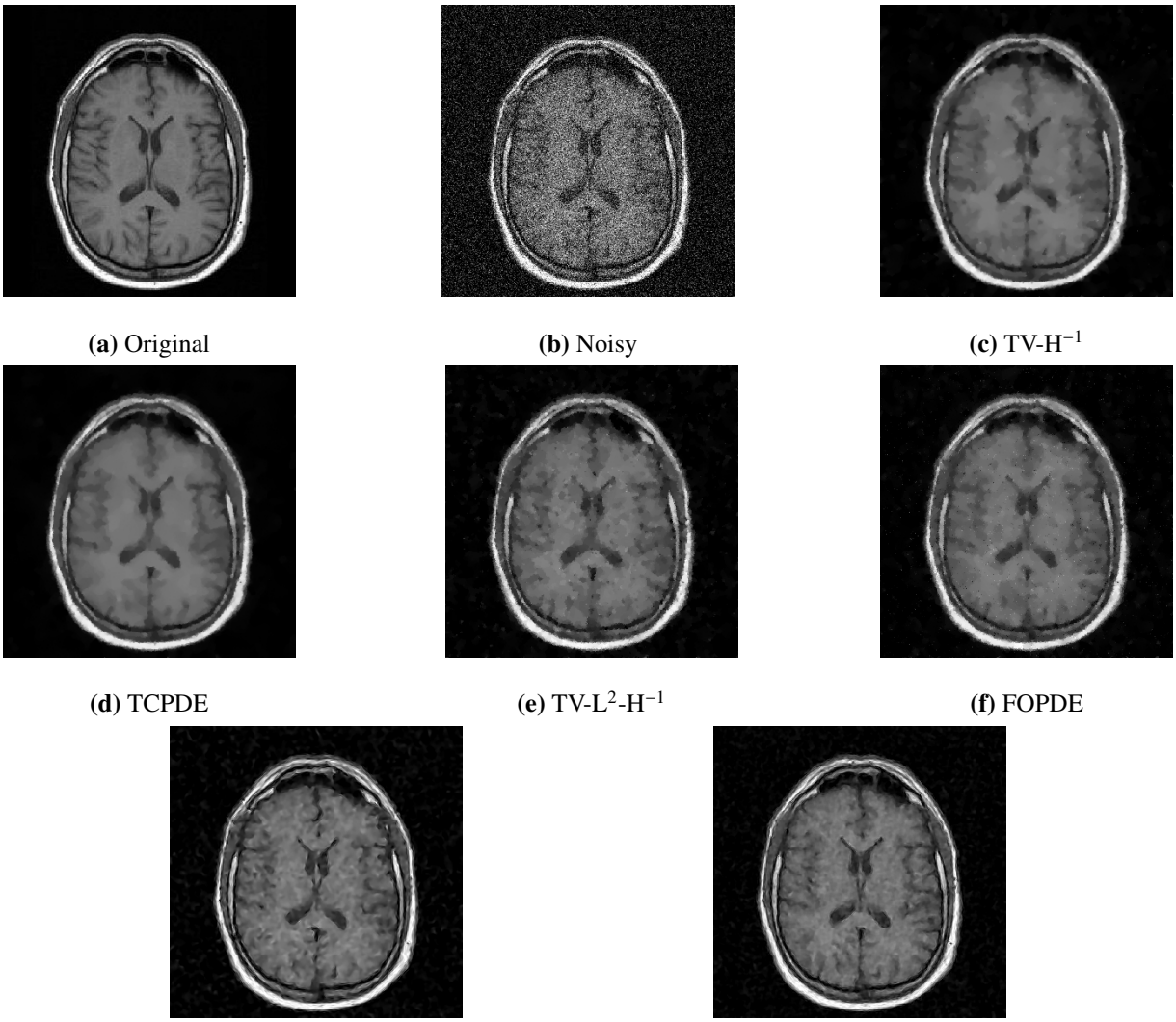

(a) Original **(b)** Noisy **(c)** TV-H^{-1}

(d) TCPDE **(e)** TV-L^2-H^{-1} **(f)** FOPDE

(g) NFAD **(h)** Our

Figure 7. *Brain* image corrupted by Gaussian noise with $\sigma = 50$ and restored by different denoising models.

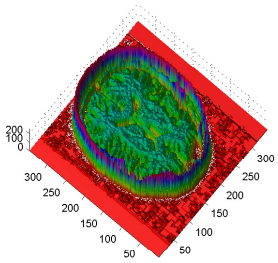

(a) Synthetic

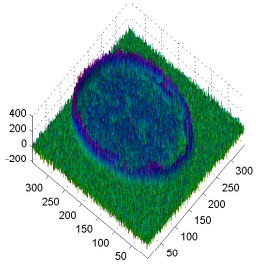

(b) Noisy

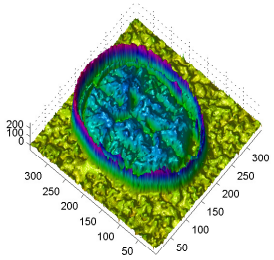

(c) TV-H^{-1}

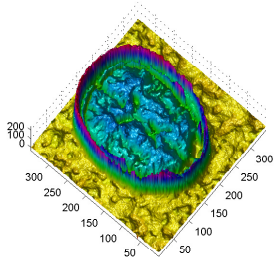

(d) TCPDE

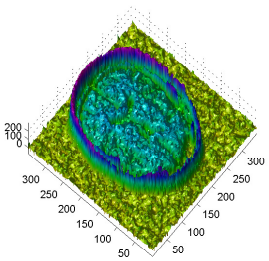

(e) TV-L^2-H^{-1}

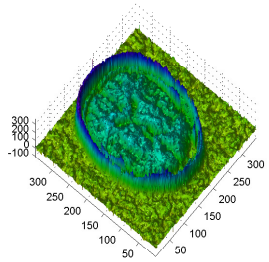

(f) FOPDE

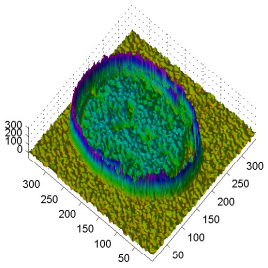

(g) NFAD

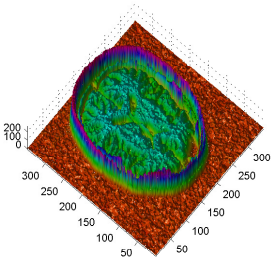

(h) Our

Figure 8. The 3D surface representations of the recovered images in Figure 7.

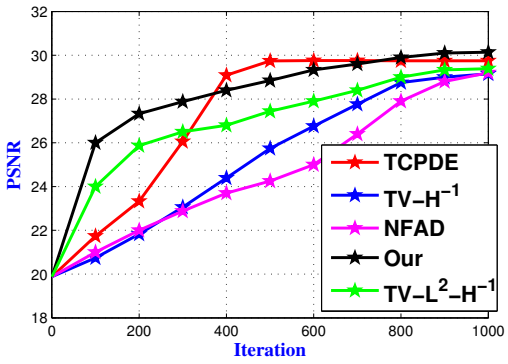

(a) PSNR (*Motif*)

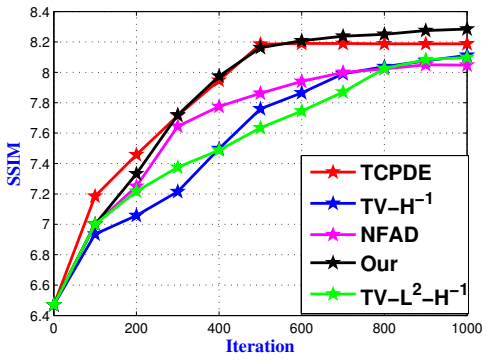

(b) SSIM (*Motif*)

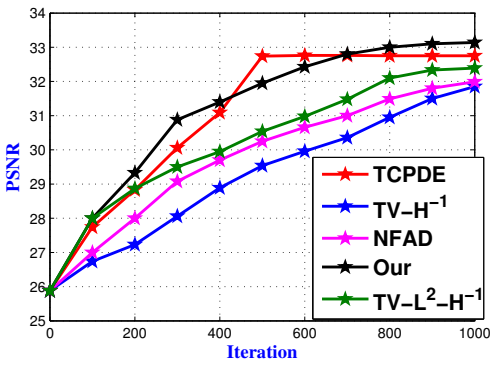

(c) PSNR (*Drop*)

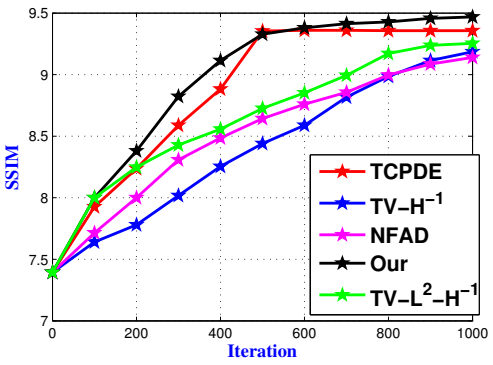

(d) SSIM (*Drop*)

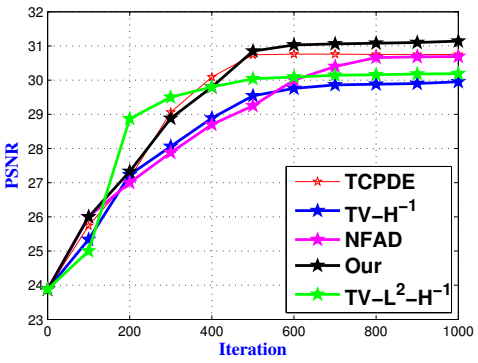

(e) PSNR (*Brain*)

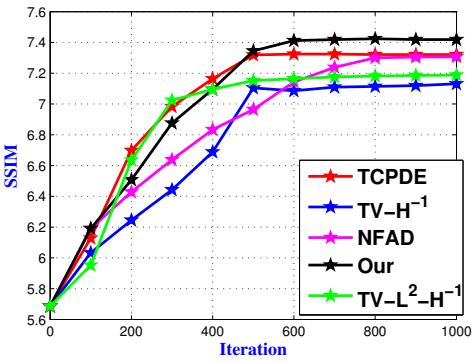

(f) SSIM (*Brain*)

Figure 9. The variation of the PSNR and SSIM values with respect to iteration number for the sequence of *Zebra*.

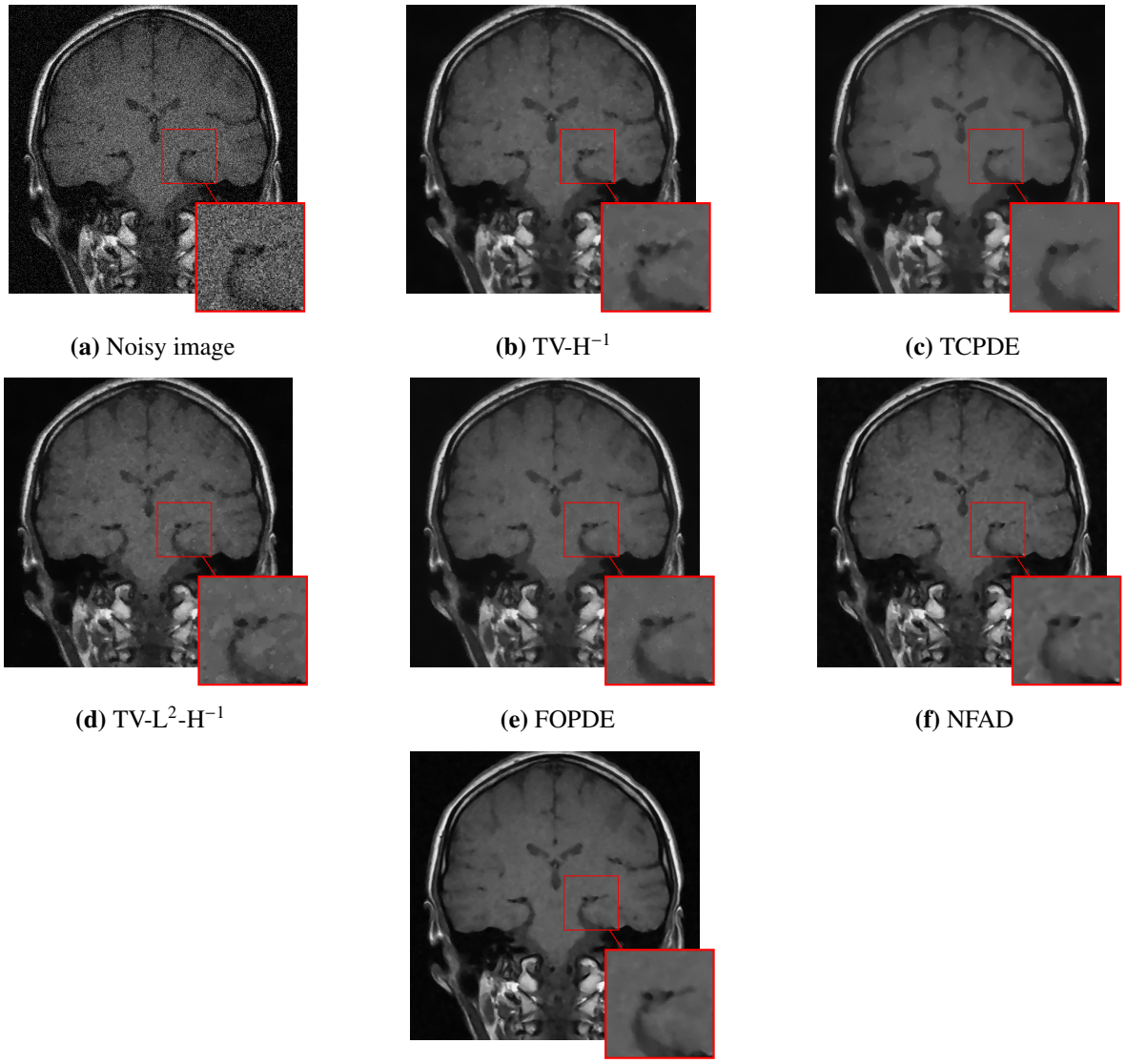

(a) Noisy image **(b)** TV-H^{-1} **(c)** TCPDE

(d) TV-L^2-H^{-1} **(e)** FOPDE **(f)** NFAD

(g) Our Method

Figure 10. Comparisons of different denoising methods of the real (*MRI Head* image). Note that the noise is unknown.

6. Conclusions

In this paper, we have proposed a coupled PDE denoising model. This PDE is based on a diffusive tensor with efficient diffusion properties along contours. The well-posedness study of the proposed PDE is also achieved using the Schauder theorem. Finally, experiment results demonstrate the ability of the proposed model compared with the results of some competitive models. Since the two parametersk_1 and k_2 affect the smoothing phenomena near strong edges, an optimization procedure will be of interest to compute these parameters, which will help the model to control the diffusion tackled by the tensor term.

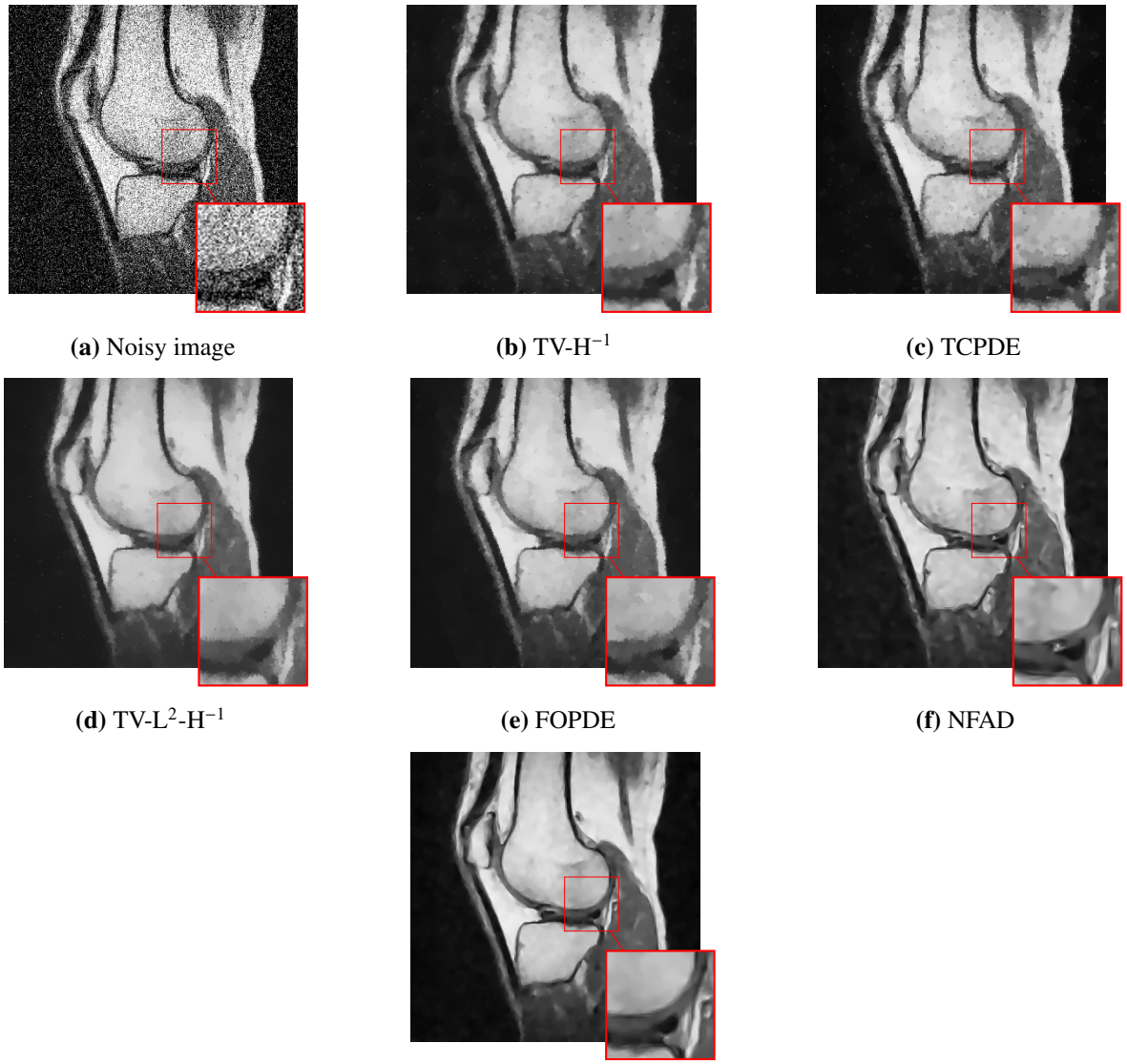

(a) Noisy image **(b)** TV-H^{-1} **(c)** TCPDE

(d) TV-L^2-H^{-1} **(e)** FOPDE **(f)** NFAD

(g) Our Method

Figure 11. Comparisons of different denoising methods (*MRI Knee* image). Note that the noise is unknown.

Acknowledgement

The authors are grateful to the two reviewers for their valuable comments, which improved the readability of this paper.

Conflict of interest

The authors declare that they have no conflict of interest.

References

1. Z. Guo, J. Yin, Q. Liu, On a reaction-diffusion system applied to image decomposition and restoration, *Math. Comput. Model.*, **53** (2011), 1336–1350. https://doi.org/10.1016/j.mcm.2010.12.031
2. Z. Guo, Q. Liu, J. Sun, B. Wu, Reaction-diffusion systems with $p(x)$-growth for image denoising, *Nonlinear Anal. Real World Appl.*, **12** (2011), 2904–2918. https://doi.org/10.1016/j.nonrwa.2011.04.015
3. A. Hadri, H. Khalfi, A. Laghrib, M. Nachaoui, An improved spatially controlled reaction–diffusion equation with a non-linear second order operator for image super-resolution, *Nonlinear Anal. Real World Appl.*, **62** (2021), 103352. https://doi.org/10.1016/j.nonrwa.2021.103352
4. M. Lysaker, A. lundervold, X. Tai, Noise removal using fourth-order partial differential equation with applications to medical magnetic resonance images in space and time, *IEEE Trans. Image Process*, **12** (2003), 1579–1590. https://doi.org/10.1109/TIP.2003.819229
5. S. G. Chang, B. Yu, M. Vetterli, Adaptive wavelet thresholding for image denoising and compression, *IEEE Trans. Image Process*, **9** (2000), 1532–1546. https://doi.org/10.1109/83.862633
6. G. Gimel'farb, *Image Textures and Gibbs Random Fields*, Kluwer Academic Publishers, 1999.
7. A. Buades, B. Coll, J. Morel, A non-local algorithm for image denoising, *IEEE Comput. Vis. Pattern Recognit*, **2** (2005), 60–65. https://doi.org/10.1109/CVPR.2005.38
8. L. Rudin, S. Osher, E. Fatemi, Nonlinear total variation based noise removal algorithms, *Physica D*, **60** (1992), 259–268. https://doi.org/10.1016/0167-2789(92)90242-F
9. R. Acar, C. Vogel, Analysis of bounded variation penalty methods for ill-posed problems, *Inverse Probl.*, **10** (1994), 1217–1229. https://doi.org/10.1088/0266-5611/10/6/003
10. A. Chambolle, P. Lions, Image recovery via total variation minimization and related problems, *Numer. Math.*, **76** (1997), 167–188. https://doi.org/10.1007/s002110050258
11. A. Hadri, A. Laghrib, H. Oummi, An optimal variable exponent model for magnetic resonance images denoising, *Pattern Recognit. Lett.*, **151** (2021), 302–309. https://doi.org/10.1016/j.patrec.2021.08.031
12. L. Vese, S. Osher, Modeling textures with total variation minimization and oscillating patterns in image processing, *J. Sci. Comput.*, **19** (2003), 553–572.
13. S. Osher, A. Solé, L. Vese, Image decomposition and restoration using total variation minimization and the H-1 norm, *Multiscale Model. Simul.*, **1** (2003), 349–370. https://doi.org/10.1137/S1540345902416247

14. Y. Meyer, *Oscillating Patterns in Image Processing and Nonlinear Evolution Equations*, in: Univ. Lecture Ser., AMS, 2002.
15. A. Atlas, M. Bendahmane, F. Karami, D. Meskine, O. Oubbih, A nonlinear fractional reaction-diffusion system applied to image denoising and decomposition, *Discrete Contin. Dyn. Syst. Ser. B*, **26** (2021), 4963. https://doi.org/10.3934/dcdsb.2020321
16. M. M. Y. Giga, P. Rybka, A duality based approach to the minimizing total variation flow in the space H^s, *Jpn. J. Ind. Appl. Math.*, **36** (2019), 261–286. https://doi.org/10.1007/s13160-018-00340-4
17. A. Halim, B. R. Kumar, A TV- L2- H- 1 PDE model for effective denoising, *Comput. Math. with Appl.*, **80** (2020), 2176–2193. https://doi.org/10.1016/j.camwa.2020.09.009
18. K. Papafitsoros, C. B. Schoenlieb, B. Sengul, Combined first and second order total variation inpainting using split bregman, *Image Process. Line*, **3** (2013), 112–136. https://doi.org/10.5201/ipol.2013.40
19. J. Weickert, *Anisotropic Diffusion in Image Processing*, Teubner, Stuttgart, 1998.
20. P. Perona, J. Malik, Scale-space and edge detection using anisotropic diffusion, *IEEE Trans. Pattern Anal. Mach. Intell.*, **12** (1990), 629–639. https://doi.org/10.1109/34.56205
21. I. El Mourabit, M. El Rhabi, A. Hakim, A. Laghrib, E. Moreau, A new denoising model for multi-frame super-resolution image reconstruction, *Signal Process.*, **132** (2017), 51–65. https://doi.org/10.1016/j.sigpro.2016.09.014
22. F. Catté, P.-L. Lions, J.-M. Morel, T. Coll, Image selective smoothing and edge detection by nonlinear diffusion, *SIAM J. Numer. Anal.*, **29** (1992), 182–193. https://doi.org/10.1137/0729012
23. E. Zeidler, *Nonlinear Functional Analysis Vol.1: Fixed-Point Theorems*, Springer-Verlag Berlin and Heidelberg GmbH and Co. K, 1986.
24. L. C. Evans, *Partial differential equations*, volume 19. Rhode Island, USA, 1998.
25. H. Attouch, G. Buttazzo, G. Michaille, *Variational analysis in Sobolev and BV spaces: applications to PDEs and optimization*, SIAM, 2014.
26. J.-P. Aubin, Un théoreme de compacité, *CR Acad. Sci. Paris*, **256** (1963), 5042–5044.
27. S. Majee, S. K. Jain, R. K. Ray, A. K. Majee, On the development of a coupled nonlinear telegraph-diffusion model for image restoration, *Comput. Math. with Appl.*, **80** (2020), 1745–1766. https://doi.org/10.1016/j.camwa.2020.08.010
28. A. Laghrib, A. Hadri, A. Hakim, An edge preserving high-order PDE for multiframe image super-resolution, *J. Franklin Inst.*, **356** (2019), 5834–5857. https://doi.org/10.1016/j.jfranklin.2019.02.032

AIMS Press